Elastic and Inelastic Collisions of Cold Spin-Polarized ^{133}Cs Atoms

Paul J. Leo, Eite Tiesinga,* and Paul S. Julienne

Atomic Physics Division, National Institute of Standards and Technology, Gaithersburg, Maryland 20899

D. K. Walter

Department of Physics, Princeton University, Princeton, New Jersey 08544

Steven Kadlecek and Thad G. Walker

Department of Physics, University of Wisconsin, 1150 University Avenue, Madison, Wisconsin 53706
(Received 23 April 1998)

We present theoretical calculations of thermally averaged elastic cross sections and spin-relaxation rate coefficients in the temperature range 0.1 to 300 μK for magnetically trapped, doubly polarized cesium atoms. The calculations reproduce the recent experimental results of Arndt *et al.* (1997) and Söding *et al.* (1998) for cases where the $a^3\Sigma_u$ ground state potential of Cs_2 possesses a large scattering length ($|A_3| > 35$ nm) and the magnitude of the second-order spin-orbit interaction is scaled to reproduce room temperature scattering data. [S0031-9007(98)06865-3]

The trapping and cooling of ground state alkali atoms are the subject of extensive experimental and theoretical interest. The low energy, long-range collisions which occur in these gases provide an ideal opportunity for studying weak atom-atom interactions, and evaporative cooling of these atoms is the demonstrated route to Bose-Einstein condensation. Bose-Einstein condensation of Rb [1], Na [2] and Li [3] atoms has led to both experimental and theoretical studies on the properties and means for manipulating coherent matter waves.

Recent experimental efforts to achieve Bose-Einstein condensation of ultracold doubly polarized cesium atoms, where both the nuclear and electron spin are aligned with the applied magnetic field B, have measured large elastic collisional cross sections [4], approaching the maximum permitted for an s-wave process, and large spin-relaxation rate coefficients [5] which are much greater than for other alkalis. At the atomic densities used in these experiments the large spin-relaxation rate coefficient turns out to inhibit the formation of a Bose condensate of doubly polarized Cs.

Spin-relaxation at room temperature and above (300–500 K) is also important to new medical imaging technology [6] that uses spin-polarized rare gas nuclei prepared by spin-exchange with spin-polarized Rb or Cs atoms [7]. In this paper we explain both ultracold [4,5] and room temperature [8,9] experimental Cs observations of elastic cross sections and spin-relaxation rate coefficients. We do this by restricting the range of scattering lengths for the $a^3\Sigma_u$ adiabatic Born-Oppenheimer (ABO) potential and including a second-order spin-orbit contribution that is significantly larger than the usual spin-spin dipole contribution.

In addition to the above described interactions, the multichannel scattering Hamiltonian for two colliding ^2S Cs atoms valid at room and ultracold temperatures requires the atomic hyperfine interaction to describe the coupling between the electronic and nuclear spin, the Zeeman interaction to describe the coupling with an external magnetic field, and the $X^1\Sigma_g^+$ ABO potential. For collisions between doubly polarized atoms, the $X^1\Sigma_g^+$ potential has little influence on the elastic cross section and the *total* spin-relaxation rate coefficient, defined by the sum of all rate coefficients from inelastic processes where one or both atoms have changed spin state. This is because the entrance channel for a collision between two doubly polarized atoms labeled a and b, with $\vec{f}_a + \vec{f}_b = 8$ and $m_a + m_b = 8$, possesses only $a^3\Sigma_u$ character and coupling to other channels, through spin-spin dipole and second-order spin-orbit interactions, is weak. Here $\vec{f}_\alpha = \vec{i}_\alpha + \vec{s}_\alpha$ denotes the total spin of atom α, where $\vec{i}_\alpha$ (magnitude $= 7/2$) is the nuclear spin and $\vec{s}_\alpha$ is the electron spin.

The $a^3\Sigma_u$ and $X^1\Sigma_g^+$ molecular potentials are based on *ab initio* calculations from [10] for internuclear separations $R < 20a_0$ ($1a_0 = 0.059177$ nm). For $R > 20a_0$ we combine the exchange potential of [11] and the long-range multipole potential including retardation corrections [12]. The potentials are not known with sufficient accuracy to yield ultracold scattering properties such as the scattering length. To obtain results consistent with the experimental data we systematically vary the $a^3\Sigma_u$ short-range potential similar to [13]. This procedure modifies the threshold phase or alternatively the position of the last bound state in the $a^3\Sigma_u$ potential. The short-range form of the $a^3\Sigma_u$ potential, $V_3(R)$, is modified using the parameter δ_3 defined by

$$V_3^{sh}(R) = V_3(R) + \delta_3 \times 10^{-5}(R - R_e)^2, \qquad R < R_e,$$

(1)

where $R_e = 11.84a_0$ is the minimum of the $a^3\Sigma_u$ potential. A near-zero energy scattering calculation for the scattering length of the V_3^{sh} potential shows a narrow

resonance in A_3 versus δ_3 at $\delta_3 = 0.92$, where the $a^3\Sigma_u$ scattering length approaches ∞ for δ_3 below 0.92 and $-\infty$ for δ_3 above 0.92. This resonance occurs as a bound state supported by V_3^{sh} moves through the dissociation threshold as the potential is made shallower. This pattern repeats itself as additional bound states are added or removed from the potential. In the following we use the scattering length A_3 to describe our results instead of the unphysical parameter δ_3. The $X^1\Sigma_g^+$ potential is modified in a similar manner but, as explained above and confirmed numerically, we find no observable dependence of the elastic cross section and the *total* spin relaxation on this parameter. Hence further discussion of the effects of the $X^1\Sigma_g^+$ potential is omitted.

For lighter alkali-dimer systems the spin-relaxation rate coefficient is likely controlled by the spin-spin dipole interaction [14]. However, in heavier atomic systems, contributions from the second-order spin-orbit interaction become important [15], such that in Rb the spin-spin dipole and second-order spin-orbit contributions were estimated to be of the same magnitude but opposite sign. Following [15] we write the second-order spin-orbit interaction as a spin-spin dipolelike term with an exponential function that is characteristic of exchange interactions. In atomic units ($m_e = c = \hbar = 1$) the effective spin-spin dipole term is then

$$H_{sd} = D(R)[s_a \cdot (3\hat{R}\hat{R} - 1) \cdot s_b]. \quad (2)$$

Here $\hat{R}$ is the direction of the internuclear axis, and

$$D(R) = -\alpha^2(1/R^3 - Ce^{-\beta(R - R_s)}), \quad (3)$$

where α is the fine structure constant. The latter term in Eq. (3) is the contribution from the second-order spin-orbit interaction. An *ab initio* calculation using only a limited number of excited states provides a second-order spin-orbit interaction with $C = 0.02249$ a.u. (1 a.u. $= 4.359745 \times 10^{-18}$ J), $\beta = 0.830a_0^{-1}$, and $R_s = 10a_0$ [15].

The zero-magnetic-field spin-relaxation cross section for optically pumped Cs atoms at room temperature is $2.0 \pm 0.4 \times 10^{-16}$ cm^2 [8] and recently remeasured to be $2.3 \pm 0.5 \times 10^{-16}$ cm^2 [9]. The precise procedure of extracting the coefficients that parametrize H_{sd} is discussed in detail in Ref. [9]. Briefly, the procedure is as follows: The need for many partial waves at room temperature suggests that a classical treatment of the collision trajectories is appropriate. Moreover, because of the few-picosecond duration of binary collisions at room temperature, the probability of spin relaxation in a single collision is small (~ 0.01) and thus second-order time dependent perturbation theory is used to calculate the cross sections. The thermally averaged cross section $\sigma_{th} = \langle v\sigma\rangle/\langle v\rangle$, with v the relative velocity, is then given by the integral over impact parameters ρ and collision energies E:

$$\sigma_{th} = 3\pi/2 \int \frac{E}{(kT)^2} e^{-E/kT} dE \int \rho\, d\rho\, |\varphi(D)|^2, \quad (4)$$

where the phase $\varphi(D)$ is the average of the spin-spin dipole and second-order spin-orbit interactions over the classical trajectory $R(t)$:

$$\varphi(D) = \frac{1}{\hbar} \int_{-\infty}^{\infty} dt\, D[R(t)]d_{00}^2[\psi(t)] \quad (5)$$

and $\psi(t)$ is the instantaneous collision angle measured with respect to the direction of ρ. The Wigner function is $d_{00}^2(\psi) = (3\cos^2\psi - 1)/2$.

Using this procedure and the *ab initio* estimates for $D(R)$, the room temperature σ_{th} is 0.11×10^{-16} cm^2, much smaller than measured in Ref. [8]. To correct for this discrepancy the magnitude C of the second-order spin-orbit interaction in Eq. (3) is scaled by a factor of 4.0 ± 0.5 to provide a calculated σ_{th} in agreement with the room temperature experiment [9]. This scaling procedure is allowed as the magnitude of the exponentially decreasing interaction $D(R)$ near the small R classical turning point ($R \approx 10a_0$) dominates the spin-relaxation rate coefficient. Note, however, that a recently observed room-T magnetic field dependence for Rb [16] and Cs may imply a somewhat smaller scaling factor. Nevertheless, we fix the scaling factor to 4.0 in the remainder of the paper.

In contrast to the room temperature calculations a quantum mechanical calculation is necessary at ultra-cold temperatures. The calculation is similar to that described in Refs. [15,17] and includes rotational, spin-spin dipole, hyperfine, and magnetic field induced Zeeman interactions using symmetrized molecular channel states. These are denoted by $|\alpha; \beta; \ell m_\ell\rangle$, where $\alpha(\beta)$ are eigenstates of the hyperfine and Zeeman interactions with projections m_a (m_b) on the space fixed direction of the magnetic field and ℓ is the orbital angular momentum of nuclear rotation with projection m_ℓ. At zero magnetic field this basis reduces to $|f_a m_a; f_b m_b; \ell m_\ell\rangle$, where f_α is the total atomic spin with projection m_α. The weak spin-dipole interactions H_{sd} couple channels with $\ell' = \ell, \ell \pm 2$ resulting in an infinite number of coupled equations. Fortunately contributions from incident channels with $\ell > 2$ are strongly suppressed at ultracold temperatures due to centrifugal barriers and quantum threshold effects, so the basis expansion can be truncated. Further, collisions between doubly polarized Cs atoms for odd partial waves are absent due to nuclear symmetry. The construction of the matrix elements and scattering equations in this "field" basis and their relation to the commonly used Hunds case (a) and (e) bases is lengthy and will be described elsewhere [18].

This set of coupled Schrödinger equations is solved for each value $M = m_a + m_b + m_\ell$, which is the only conserved quantum number for collisions in a magnetic field, using computer codes based on the Gordon algorithm [19]. This potential following algorithm uses large steps, where the intermolecular potential is slowly varying, making it particularly suitable for the study of ultracold collisions, where integration out to $R > 10\,000a_0$ may be required. Scattering matrix elements for each scattering length are calculated at over 100 energies between $E/k_b = 0.001$ and 1300 μK (where k_b is Boltzmann's

constant) to provide thermalized elastic cross sections σ_{th} and spin-relaxation rate coefficients $K(T) = \langle v\sigma \rangle$ between 1 and 300 μK converged to 2%.

In Figs. 1 and 2 we compare our theoretical calculations for the elastic cross section at 0.4 mT and spin-relaxation rate coefficient at 0.15 mT with the experimental results of [4] and [5], respectively. The theoretical results include all s- and d-wave contributions and require the solution of 28, 16, 9, 3, and 1 coupled equations for a total $M = 6$, 7, 8, 9, and 10, respectively. The results for different V_3^{sh} potentials with negative/positive scattering lengths are denoted by dashed/solid lines. Calculations using a shallower exchange potential or using a different long-range dispersion potential, such as that of [20] which possesses a van der Waals C_6 coefficient 5% larger than that of [12], provide cross sections within 10% of the results presented here. The weak dependence of cross sections on C_6 was also found in Ref. [13] when calculating the ultracold Cs clock shift.

In Fig. 1 the elastic cross sections for potentials with scattering lengths of magnitudes less than $250a_0$ display typical Wigner-threshold behavior for s-wave scattering at temperatures less than 5 μK, whereby the elastic cross section is a constant given by $\sigma = 8\pi A_3^2$. The low energy s-wave elastic cross section including higher-order terms in the collision energy [21] behaves as

$$\sigma = \frac{8\pi A_3^2}{(1 - \frac{1}{2} k^2 A_3 r_0)^2 + k^2 A_3^2},\qquad(6)$$

where $\hbar^2 k^2 / 2\mu$ is the asymptotic kinetic energy, μ is the reduced mass, and r_0 is the effective range of the

potential. Thus the cross sections for potentials with larger scattering lengths reach threshold behavior, where $kA_3 \ll 1$, at much smaller temperatures.

For the unthermalized elastic cross sections the contribution from d-wave scattering rises rapidly for $E/k_b > 75$ μK while the contribution from s-wave scattering decreases to zero at $E/k_b \approx 200$ μK. This rapid decrease of the s-wave contribution is not compensated by the increase in the d-wave contribution. The end result appears in Fig. 1 as a broad minimum in the total thermalized elastic cross section around ≈ 150 μK. An exception to this behavior is the elastic cross section for $A_3 = 100a_0$. In this instance, five distinct d-wave shape resonances, associated with the five doubly polarized channels labeled $|4,4;4,4;2m_\ell\rangle$ in the field free basis, occur between $E/k_b = 20$ and 30 μK. In the thermalized cross sections these narrow resonances are broadened into the feature from $10-80$ μK. In Fig. 2 the same resonances appear as a broad feature from 1 to 500 μK for $A_3 = 100a_0$.

For all scattering lengths the g-wave contribution to the unthermalized elastic cross section is less than 0.5% for energies $E/k_b < 1000$ μK. Above 1000 μK the g wave can contribute up to 5% of the total cross sections. However, when calculating the thermalized cross sections up to 300 μK, these high contributions are strongly suppressed by the Maxwell distribution.

The calculations, as noted above, are performed at $B = 0.4$ and 0.15 mT used in [4] and [5], respectively. Our calculations show that σ_{th} and K are almost independent of B from 0.1 to 10 mT for all $a^3\Sigma_u$ scattering lengths tested. The elastic cross sections remain constant to within 1% while the spin-relaxation rate coefficients
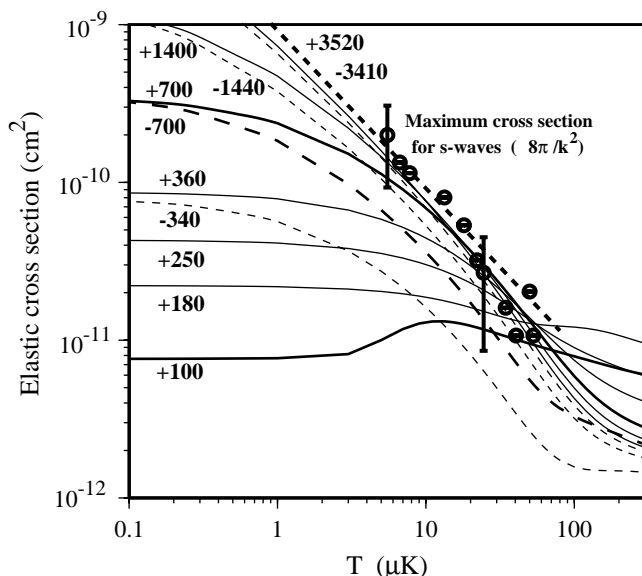

FIG. 1. Elastic cross section versus temperature for doubly polarized Cs atoms. The solid/dashed curves represent theoretical results for various V_3^{sh} potentials with positive/negative scattering lengths. The experimental results of [4] are denoted by (⊖) with experimental errors estimated at two temperatures. The maximum allowed cross section for s waves is given by the short-dashed line.
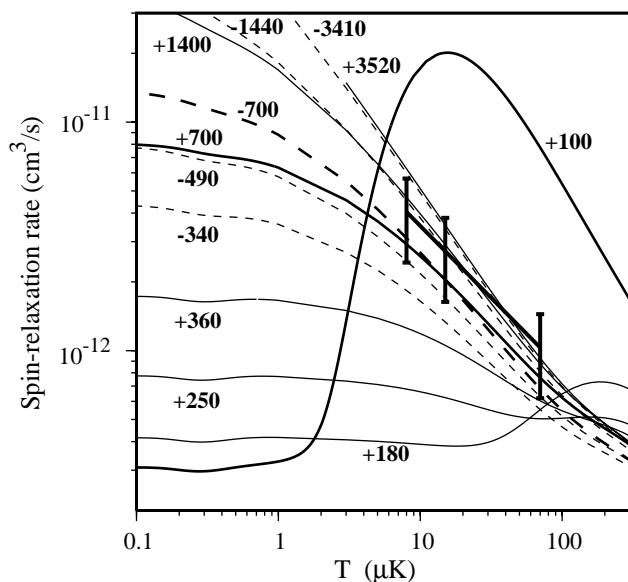

FIG. 2. Spin-relaxation rate coefficient versus temperature for doubly polarized Cs atoms. The solid/dashed curves represent theoretical results for various V_3^{sh} potentials with positive/negative scattering lengths. The experimental results [5] are given as a thick solid line with experimental error bars.

first increase by 5% between $B = 0$ and $B = 2.5$ mT before becoming constant from 2.5 to 10 mT. The slow increase in the spin-relaxation rate coefficient from 0 to 2.5 mT is due to d-wave centrifugal barriers in exit channels with dissociation energies that lie just below that for the s-wave doubly polarized incident channel. At zero field these exit channels are degenerate with the incident channel and then inelastic processes into these states are suppressed as collision energies are smaller than the height of the d-wave barrier and penetration through the barrier is minimal. For small magnetic fields, however, the Zeeman interaction lowers the internal energy of these states with respect to the entrance channel, and at 2.5 mT the incident channel energy rises above the d-wave barrier of these exit channels and their contribution to spin relaxation is no longer suppressed.

Exceptions to this uniform behavior are found in cross sections that possess d- or g-wave exit channel resonances. These narrow shape resonances are particularly sensitive to the position of the virtual bound states supported by the scattering potential, which shift relative to each other as the magnetic field is increased. These resonances are observed for small scattering lengths, $A_3 < 150a_0$, but in general the cross sections cannot be modified significantly by varying the magnetic field.

In Fig. 1 the experimental results of [4] are given assuming an average of 10.7 collisions for the Cs atoms to reach thermalization, a result which they obtain using a Monte Carlo simulation of their Cs trap. The comparison between our theory and the experimental results is favorable for potentials possessing scattering lengths with magnitudes in excess of $600a_0$. A further reduction in the range of possible $a^3\Sigma_u$ scattering lengths is hampered because the cross sections for potentials with large scattering lengths ($>1000a_0$) do not deviate from the maximum σ until temperatures are less than 1 μK, where there is no experimental data.

Figure 2 describes the thermalized spin-relaxation rate coefficients where the magnitude C of the *ab initio* second-order spin-orbit interaction in Eq. (3) is scaled by a factor of 4 to fit the room-T relaxation data. Within the existing experimental temperature range, the theoretical results are found to scale as C^2 to better than 3%. Therefore any error in scaling this interaction results in an overall shift of the theoretical curves in Fig. 2, but leave the slopes unaffected. Within the uncertainties of the scaling factor, determined previously from room temperature data, the potentials with $|A_3| > 600a_0$ are consistent with current experimental data. Elastic cross sections and spin-relaxation rate coefficients, produced by potentials with small scattering lengths $\approx 100a_0$ that possess a d-wave resonance, completely fail to reproduce the experimental results.

The present calculations are the first to include a realistic second-order spin-orbit interaction in ultracold Cs-Cs scattering and demonstrate that it significantly modifies the spin-relaxation rate coefficient. With a second-order spin-orbit interaction, appropriately scaled to reproduce room temperature scattering data, the thermalized spin-relaxation and elastic cross sections at ultracold temperature are both reproduced with $|A_3| > 600a_0$. From experimental measurements of the ultracold Cs clock shift at ≈ 1.5 μK [13], we have estimated the $a^3\Sigma_u$ scattering length to be between $-200a_0$ and $-1100a_0$. These calculations require detailed information of both the $X^1\Sigma_g$ and $a^3\Sigma_u$ potentials. The calculations performed here depend only upon the $a^3\Sigma_u$ potential and do not exclude large positive scattering lengths. A survey of the magnetic field dependence of the cross sections indicates that the large spin-relaxation rate coefficient cannot be modified significantly using magnetic fields up to 0.01 T.

*Permanent address: Department of Chemistry and Biochemistry, Univ. of Maryland, College Park, MD 20742

[1] M. H. Andersen *et al.,* Science **269**, 198 (1995).
[2] K. B. Davis *et al.,* Phys. Rev. Lett. **75**, 3969 (1995).
[3] C. C. Bradley, C. A. Sackett, and R. G. Hulet, Phys. Rev. Lett. **78**, 985 (1997).
[4] M. Arndt *et al.,* Phys. Rev. Lett. **79**, 625 (1997).
[5] J. Söding *et al.,* Phys. Rev. Lett. **80**, 1869 (1998).
[6] J. MacFall *et al.,* Radiology **200**, 553 (1996).
[7] T. G. Walker and W. Happer, Rev. Mod. Phys. **69**, 629 (1997).
[8] N. D. Bhaskar *et al.,* Phys. Rev. Lett. **44**, 930 (1980).
[9] D. K. Walter, W. Happer, and T. G. Walker (to be published); S. Kadlecek, T. G. Walker, and D. K. Walter (to be published).
[10] M. Krauss and W. J. Stevens, J. Chem. Phys. **93**, 4236 (1990).
[11] W. Weickenmeier *et al.,* J. Chem. Phys. **82**, 5354 (1985).
[12] M. Marinescu, J. F. Babb, and A. Dalgarno, Phys. Rev. A **50**, 3096 (1994).
[13] B. J. Verhaar, K. Gibble, and S. Chu, Phys. Rev. A **48**, R3429 (1993).
[14] B. H. Bransden and C. J. Joachain, *Physics of Atoms and Molecules* (Longmans, New York, 1983), p. 366.
[15] F. Mies *et al.,* J. Res. Natl. Inst. Stand. Technol. **101**, 521 (1996).
[16] S. Kadlecek, L. W. Anderson, and T. G. Walker (to be published).
[17] H. T. C. Stoof, J. M. V. A. Koelman, and B. J. Verhaar, Phys. Rev. B **38**, 4688 (1988).
[18] C. J. Williams *et al.,* (to be published).
[19] F. H. Mies, Phys. Rev. A **7**, 957 (1973).
[20] S. H. Patil and K. T. Tang, J. Chem. Phys. **106**, 2301 (1997).
[21] N. F. Mott and H. S. W. Massey, *The Theory of Atomic Collisions* (Clarendon Press, Oxford, 1965), p. 47.